Electron-impact ionization of highly excited hydrogenlike ions in a collinear *s*-wave model

T. Topçu,[1] M. S. Pindzola,[1] C. P. Ballance,[2] D. C. Griffin,[2] and F. Robicheaux[1]
[1]*Department of Physics, Auburn University, Alabama 36849-5311, USA*
[2]*Department of Physics, Rollins College, Winter Park, Florida 32789, USA*
(Received 29 June 2006; published 15 December 2006)

We report results from collinear time-dependent close-coupling (TDCC), distorted-wave (DW), and *R* matrix with pseudostates calculations for the electron-impact ionization of H-like ions up to $Z=6$ within an *s*-wave model. We compare the results of these calculations with those from a collinear classical trajectory Monte Carlo calculation to investigate the correspondence between the quantal and classical ionization probabilities as the principal quantum number of the initial state increases. In these model calculations, the electron-electron interaction is represented by the collinear *s*-wave potential given by $1/(r_1+r_2)$. We study the ionization probability from the ground state and highly excited states up to $n=25$ as a function of incident energy and the charge of the ion. We show that the fully quantal ionization probability converges to the classical results rapidly for hydrogen. The higher ion stages exhibit much slower convergence with respect to n. We observed good agreement between the DW and TDCC for the n range we have considered for B^{4+}. For hydrogen, we found fairly good agreement between the DW and TDCC for the ground state, but the worsening disagreement with increasing n. There is reasonable agreement between the results from the *R*-matrix calculations and the results from the TDCC calculations confirming the convergence of the TDCC results.

DOI: 10.1103/PhysRevA.74.062708 PACS number(s): 34.10.+x, 34.60.+z, 34.80.Dp, 34.80.Kw

I. INTRODUCTION

According to the Bohr correspondence principle, the quantum mechanical description of a physical system should yield classical dynamics in the appropriate limit. Although there is no common agreement on how this limit should be defined, the most widely accepted definition is in terms of large quantum numbers. The classical-quantum correspondence in this context has been subject of many theoretical studies [1–3] as well as to experiments with Rydberg atoms [4]. There are systems which were found to violate the correspondence principle [2] as well as ones that fulfilled it exactly without taking any limits [3]. In a recent experiment by Nagesha and MacAdam [5], highly excited Na Rydberg atoms with principal quantum numbers of $n=35-51$ revealed quite large electron-impact ionization cross sections compared to a formula designed to estimate the ionization cross sections out of excited states within an *n*-manifold, and a theory [6] based on low-*n* data. The discrepancy between the experiment and the theoretical models suggests that electron impact ionization from Rydberg states may exhibit peculiar dynamics.

Ionization by electron impact out of highly excited states would be expected to yield cross sections that are consistent with classical models at sufficiently high quantum numbers. However, the convergence to classical dynamics may very well depend on the properties of the atom, such as its ionic charge or the strength that the electron interacts with an external system or source. The question as to how well the atomic electron can be described classically as the principal quantum number increases is the focus of the present study. We investigate electron-impact ionization of H-like ions up to $Z=6$ for various electron-impact energies. We performed calculations up to $n=25$ in initial principal quantum number using a time-dependent close-coupling (TDCC) method in a collinear *s*-wave model. We contrast results of these calculations with those from collinear *s*-wave classical trajectory Monte Carlo (CTMC), distorted-wave (DW), and *R*-matrix calculations.

Although electron-impact ionization has been covered extensively in the literature (e.g., see Refs. [7–9], and references therein), there has only been a few non-perturbative calculations for the electron-impact ionization from low excited states [10–12]. A recent paper by Griffin *et al.* [13] presents results from a series of nonperturbative quantal calculations for electron-impact ionization from H, Li^{2+}, and B^{4+} up to $n=4$ in comparison to fully three dimensional CTMC and perturbative distorted-wave calculations. Their nonperturbative calculations employed primarily the *R*-matrix with pseudostates (RMPS) method whose results compared very well with those from their TDCC calculations for ionization from selected excited states. Using the nonperturbative results as benchmarks, their study indicated that the CTMC results were reasonably accurate for hydrogen, but for the ions the CTMC results were too large and did not improve with the principal quantum number.

Electron-impact scattering from hydrogenlike ions is also an important atomic process for modeling of tokamak plasmas and performing plasma diagnostics. Therefore it is important to have ionization data accurate enough to satisfactorily model and diagnose laboratory plasmas. Usually, the cross sections for electron-impact ionization are obtained from fully quantal calculations for ionization from the lowest states and from classical calculations for ionization from highly excited states [14]. It has been shown [15] that for denser plasmas the effective ionization rate changes substantially when contributions through higher n levels are included in addition to the ground and metastable states. The sensitivity of the plasma models to the atomic data illustrates the need for the investigation of the extent to which the classical cross sections are accurate.

Since both the number of n, l terms and the size of the target increase rapidly with principal quantum number, the

computational resources required to study ionization out of highly excited states become prohibitively large for a full three-dimensional model. Therefore, in this study, we restrict ourselves to the collinear *s*-wave model where both electrons move on a straight line. It has been shown that this model includes the essential physics of the ionization process close to the threshold [16–18] and yields the correct Wannier threshold law for single ionization, i.e., $\sigma \sim E^{1.128}$. The interaction potential between the electrons is $1/(r_1+r_2)$ which we refer to as the collinear *s*-wave potential.

In the next section, we discuss the theoretical methods employed. In Sec. III, we present our results and in Sec. IV, we discuss their signficance. We use atomic units throughout this paper.

II. THEORY

We first describe the collinear *s*-wave TDCC model and discuss the various convergence checks performed. Next we discuss the collinear *s*-wave CTMC, DW, and RMPS methods that we employed. Since the accuracy of the results is important, we make special effort to discuss the methods we used to insure convergence.

A. The time-dependent wave packet method using the collinear *s*-wave model

In the collinear *s*-wave model where both electrons move on a straight line, the Hamiltonian reads [19]

$$H = \sum_{\alpha=1}^{2} \left(\frac{p_\alpha^2}{2} - \frac{Z}{r_\alpha} \right) + \frac{1}{r_1 + r_2}. \tag{1}$$

If the *H*-like ion is initially in the *ns* state, the symmetrized initial wave function at $t=0$ is

$$\psi(r_1, r_2, t=0) = \frac{1}{\sqrt{2}} [\varphi_{ns}(r_1) G_{ks}(r_2) + \varphi_{ns}(r_2) G_{ks}(r_1)] \tag{2}$$

where φ_{ns} is an eigenstate of the *H*-like ion and G_{ks} is the Gaussian representing the incoming electron of energy $E = k^2/2$ and momentum k. It is given by

$$G_{ks}(r) = e^{-i\phi(r)} e^{-[\Lambda/(r_f - r_0)]^2 [r - (1/2)(r_f + r_0)]^2}, \tag{3}$$

where $r_0 = 2n^2$ and the constant Λ is chosen such that $e^{-(\Lambda/2)^2} \ll 1$ and $G_{ks}(r)$ can be considered to be zero at $r=r_0$ and $r=r_f$. In our calculations, we have taken Λ to be 12. To reduce the energy spread of the packet due to the phase accumulations, the WKB phase $\phi(r)$ is evaluated as

$$\phi(r) = \int_0^r \sqrt{2[E + (Z-1)/r']}\, dr'. \tag{4}$$

The wave packet is discretized on a two-dimensional square root mesh where $r_j = j^2 \delta r$ with $\delta r = r_f/N^2$. The maximum grid spacing on this mesh can be evaluated by $\delta r_{\max} = (2N-1)\delta r$ and is two times larger than that for a linear mesh.

Time propagation of the Schrödinger equation is carried out by means of lowest order split operator technique

$$\psi(t+\delta t) = \exp\left(-i \frac{\delta t}{2(r_1 + r_2)} \right) \exp(-iH_2 \delta t) \times \exp(-iH_1 \delta t) \exp\left(-i \frac{\delta t}{2(r_1 + r_2)} \right) \psi(t), \tag{5}$$

where $H_\alpha = p_\alpha^2/2 - Z/r_\alpha$ and $(\alpha = 1, 2)$. Using the lowest order Padè approximation for the exponential one particle operators $\exp(-iH_\alpha \delta t/2)$, the time propagation scheme given by Eq. (5) becomes

$$\psi(t+\delta t) = \exp\left(-i \frac{\delta t}{2(r_1 + r_2)} \right) \left[\frac{1 - iH_2 \delta t/2}{1 + iH_2 \delta t/2} \right] \times \left[\frac{1 - iH_1 \delta t/2}{1 + iH_1 \delta t/2} \right] \exp\left(-i \frac{\delta t}{2(r_1 + r_2)} \right) \psi(t). \tag{6}$$

The numerical error for this lowest order Padè approximation scales as δt^3 and the approximated operator is exactly unitary. The probability of finding both electrons in the continuum at time t is calculated by making use of the *bound* states φ_{ns},

$$\mathcal{P}_{2e^-}(t) = 1 - 2 \sum_n \int \left| \int \psi(r_1, r_2, t) \varphi_{ns}(r_1) dr_1 \right|^2 dr_2 + \sum_n \sum_m \left| \int \int \psi(r_1, r_2, t) \varphi_{ns}(r_1) \varphi_{ms}(r_2) dr_1 dr_2 \right|^2, \tag{7}$$

provided that the wave function is normalized to unity [20]. The ionization cross section σ_{2e^-} is calculated from the ionization probability using $\sigma_{2e^-} = (\pi/k^2)\mathcal{P}_{2e^-}$.

To increase the accuracy of the computed projections, we have calculated the eigenstates in a box two times larger than the box in which $\psi_{j,k}$ is discretized. This gives a finer spacing of states in energy and decreases the effect of a finite box. In discretization of the Hamiltonian on the square root mesh, we have used a three point differencing scheme for the second derivatives. The action of $p^2/2$ on the eigenstate φ_j is calculated as [21]

$$\frac{1}{2} p^2 \varphi_j = - \frac{\varphi_{j-1}}{\sqrt{(r_j - r_{j-1})(r_{j-1} - r_{j-2})}(r_j - r_{j-1})} + \frac{\varphi_j}{(r_{j+1} - r_j)(r_j - r_{j-1})} - \frac{\varphi_{j+1}}{\sqrt{(r_{j+1} - r_j)(r_j - r_{j-1})}(r_{j+1} - r_j)}, \tag{8}$$

where $\varphi_j = R_j/\sqrt{\delta r_j}$ and R_j is the actual radial orbital. The advantage of using a square root mesh is that it enables us to employ much larger boxes than the uniform mesh does. To check the effect of using a square root mesh on our results, we have also performed a few trial calculations on a uniform mesh and compared the results with those from the square root mesh calculations. We did not see any significant differences in the projected probabilities.

We use scaled units to describe the electron-impact energy E in our calculations. Energies of the incoming electron are

chosen in multiples of the binding energy of the initial state. The energy of the incoming electron is therefore defined by $E=[Z^2/(2n^2)]E_{sc}$, where we call E_{sc} the scaled electron-impact energy.

We have checked convergence of the TDCC results with respect to box size r_f, number of points N, and time step δt for the time propagation. For example, for an atom in an initial state with $n=12$ and an incoming electron with scaled energy $E_{sc}=9.5$, the projected ionization probability for all Z in a 2250 (a.u.) box with 2500 points remains well within a percent if one increases the number points to 5000 while keeping r_f fixed. When the number of points is kept fixed at 2500 and the box size is doubled, the probability changes by $\sim 2\%$ for $Z=1$. In cases of $Z=3$ and $Z=5$, the differences are within $\sim 1\%$. When both r_f and N are doubled to 4500 and 5000, respectively, the results were within $\sim 3\%$ of the $(r_f,N)=(2250,5000)$ results for $Z=1$. For $Z=5$ the difference was $\lesssim 1\%$. We have found that for sufficiently high n, amplitudes for superelastic scattering down to low-n states are very small, enabling us to employ large δr_{max} and r_f. We carried out similar analyses for all the initial states and several ion stages in our calculations and the results we present are converged within a few percent.

To be able to use the same converged box parameters and time steps for all Z, we scale the length and time according to $r_j=\zeta_j/Z$ and $t=\tau/Z^2$. The full time-dependent Shrödinger equation that needs to be solved is

$$i\frac{\partial}{\partial t}\psi=\left[\sum_{\alpha=1}^{2}\left(\frac{1}{2}\frac{\partial^2}{\partial r_\alpha^2}-\frac{Z}{r_\alpha}\right)+\frac{1}{r_1+r_2}\right]\psi(r_1,r_2). \tag{9}$$

After scaling and dividing through by Z, Eq. (9) becomes

$$i\frac{\partial}{\partial \tau}\psi=\left[\sum_{\alpha=1}^{2}\left(\frac{1}{2}\frac{\partial^2}{\partial \zeta_\alpha^2}-\frac{1}{\zeta_\alpha}\right)+\frac{1}{Z(\zeta_1+\zeta_2)}\right]\psi(\zeta_1,\zeta_2) \tag{10}$$

which is equivalent to the hydrogen problem in scaled coordinates and time, except the scaled electron-electron interaction potential is now $1/[Z(\zeta_1+\zeta_2)]$. In the same manner, scaling the time independent Schrödinger equation for the evaluation of the eigenenergies and the eigenstates, we solve the equation

$$-\frac{1}{2}\frac{\partial^2\phi(\zeta)}{\partial\zeta^2}-\frac{\phi(\zeta)}{\zeta}=\tilde{\epsilon}\phi(\zeta) \tag{11}$$

with the Z-scaled energy $\tilde{\epsilon}=\epsilon/Z^2$. Note that with the use of the Z-scaled potential, the electron-impact energy becomes $E=[1/(2n^2)]E_{sc}$.

For B^{4+}, for an initial state with $n=4$ and with a scaled impact energy of $E_{sc}=9.5$, the difference in the ionization probability between the calculations using the collinear s-wave potential and the Z-scaled collinear s-wave potential is found to be within a percent.

B. Classical trajectory Monte Carlo method

In the CTMC method, we solved the classical equations of motion to compute the classical probability for ionization. The classical equations of motion scale. This means the ionization probability in the collinear s-wave model only depends on Z and on the ratio of the kinetic energy of the incident electron to the binding energy of the bound electron; we define this to be the scaled incident energy E_{sc}. In addition to Z and E_{sc}, the TDCC results depend on the binding energy of the target state.

The length and time scalings are

$$r=\rho\frac{Z}{E_b},\quad t=\tau\frac{Z}{E_b^{3/2}}, \tag{12}$$

where E_b is the binding energy of the attached electron. For this choice of scaling, the scaled energy of the bound electron is -1 and the incident energy is E_{sc}. A bound energy of -1 corresponds to $n=1/\sqrt{2}$ and a classical period of $2\pi n^3=\pi/\sqrt{2}$.

With this scaling the fully three dimensional equations of motion become

$$\frac{d\vec{\nu}_1}{d\tau}=-\frac{\vec{\rho}_1}{\rho_1^3}+\frac{1}{Z}\frac{\vec{\rho}_{12}}{\rho_{12}^3},\quad \frac{d\vec{\rho}_1}{d\tau}=\vec{\nu}_1, \tag{13}$$

$$\frac{d\vec{\nu}_2}{d\tau}=-\frac{\vec{\rho}_2}{\rho_2^3}-\frac{1}{Z}\frac{\vec{\rho}_{12}}{\rho_{12}^3},\quad \frac{d\vec{\rho}_2}{d\tau}=\vec{\nu}_2, \tag{14}$$

where $\vec{\rho}_{12}=\vec{\rho}_1-\vec{\rho}_2$. For the collinear s-wave model, the scaled equations of motion are

$$\frac{d\nu_1}{d\tau}=-\frac{1}{\rho_1^2}+\frac{1}{Z}\frac{1}{(\rho_1+\rho_2)^2},\quad \frac{d\rho_1}{d\tau}=\nu_1, \tag{15}$$

$$\frac{d\nu_2}{d\tau}=-\frac{1}{\rho_2^2}+\frac{1}{Z}\frac{1}{(\rho_1+\rho_2)^2},\quad \frac{d\rho_2}{d\tau}=\nu_2, \tag{16}$$

with the additional condition of an infinitely hard wall at a small, positive value of ρ, after which the electron cannot move any closer to $\rho=0$. The infinitely hard wall reverses the sign of the velocity and keeps both electrons at positive ρ. The position of the wall affects the ionization probability, but the effect decreases as the wall moves closer to $\rho=0$. We chose a position 5×10^{-5}, where the ionization probability was changed by much less than a percent. Note that the nuclear charge Z manifests itself in the scaled equations of motion by multiplying the electron-electron interaction by $1/Z$. From this it is clear that the ionization (which depends on the electron-electron interaction) decreases with increasing Z.

If there were no scattering, the bound electron would be limited to a region $0<\rho\leqslant 1$. The initial conditions of the bound electron were chosen to give a microcanonical ensemble. For the collinear case, this means the starting position and velocity can be specified by a single random parameter η in the range $0\leqslant\eta\leqslant 1$; if η is chosen correctly the distribution is flat in η. The microcanonical ensemble is given where the parameter η is the fraction of a period of the bound motion and the position and velocity at $\eta=0$ is taken to be the outer turning point, $\rho=1,\nu=0$. The initial conditions for the fully three dimensional case are somewhat more complicated but are well known (e.g., see Ref. [22]).

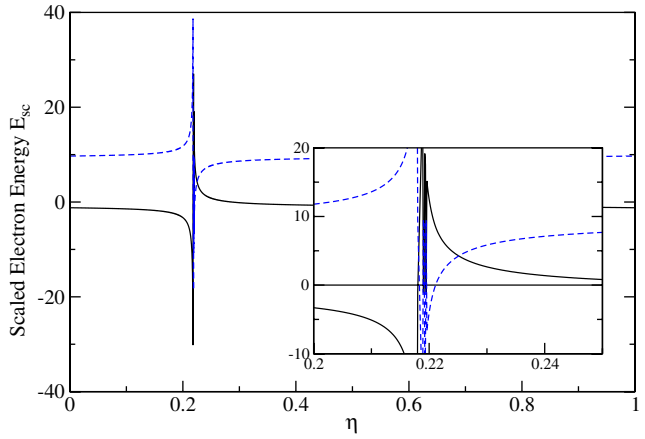

FIG. 1. (Color online) Scaled final energy of the classical bound (solid curve) and incoming (dashed curve) electrons versus the initial phase, η, of the bound electron. The initial position and velocity of the electron ρ and ν are found by solving the classical equations of motion for a time given by η times the Rydberg period with $\rho(0)=1$ and $\nu(0)=0$. This graph shows the result for $Z=1$ and $E_{sc}=9.5$. Note that the width of the region where η is positive for both electrons (shown in the inset) is the ionization probability.

The incident electron is started at a distance $\rho_2=100$. In the collinear s-wave calculation, the initial velocity is $\nu_2=-\sqrt{2(E_{sc}-V_0)}$, where $V_0=-1/\rho_2(0)+(1/Z)\{1/[\rho_1(0)+\rho_2(0)]\}$ is the initial potential energy for electron 2. With this definition, the total energy is exactly $E=-1+E_{sc}$. We run the trajectories until at least one electron reaches the distance $\rho=120$, at which point the energies of the electrons are computed. The η range for which the energies of both of the electrons are positive gives the ionization probability $\mathcal{P}_{2e^-}$, which is converted to cross section via $\sigma_{2e^-}=(\pi/k^2)\mathcal{P}_{2e^-}$. The initial conditions for the three dimensional calculation is similar but includes the impact parameter of the incident electron.

For the collinear s-wave model, the initial conditions only depend on one parameter η. Therefore, it makes physical sense to examine the energies of the electrons versus η. In Fig. 1, we show the energies of the two electrons (solid and dashed curves) versus η for $Z=1$ and $E_{sc}=9.5$. It is clear that relatively little energy is transferred to the bound electron (solid curve) except in a region near $\eta=0.25$ which is shown as an inset. The region where both energies are positive corresponds to ionization. Because the microcanonical distribution is flat in η and the range of η is one, the fraction ionized simply corresponds to the range of η where both energies are positive. The energies versus η have similar types of shape for all Z. There is a small region where substantial energy exchange can occur; the width of the region decreases with increasing Z. The large energy transfer occurs when the incoming electron and the bound electron are moving in the same direction near the nucleus; for this type of motion, the incoming electron can do substantial work on the bound electron, giving it enough energy to ionize.

C. Collinear distorted-wave method

In the collinear s-wave distorted-wave theory, the ^1S cross section for single ionization of a hydrogenic ion is given by

$$\sigma=\frac{32}{k_i^3}\int_0^{E/2}\frac{d(k_e^2/2)}{k_e k_f}[\mathcal{R}(k_e s,k_f s;ns,k_i s)+\mathcal{R}(k_f s,k_e s;ns,k_i s)]^2, \tag{17}$$

where the linear momenta (k_i,k_e,k_f) correspond to the incoming, ejected, and outgoing electron, respectively. The direct radial matrix element is

$$\mathcal{R}(k_e s,k_f s;ns,k_i s)=\int_0^\infty dr_1\int_0^\infty dr_2 \times\frac{P_{k_e s}(r_1)P_{k_f s}(r_2)P_{ns}(r_1)P_{k_i s}(r_2)}{r_1+r_2} \tag{18}$$

with a similar expression for the exchange term. The radial distorted waves needed to evaluate the radial matrix elements are all Coulomb waves [23].

D. Collinear *R*-matrix method

In the collinear s-wave R-matrix method [24], symmetrized product states of single-particle orbitals generated by the diagonalization of the one electron Hamiltonian

$$h(r)=\frac{p^2}{2}-\frac{Z}{r}, \tag{19}$$

are used to span the basis for the diagonalization of the two electron Hamiltonian

$$\mathcal{H}_R=H(r_1,r_2)+\frac{1}{2}\delta(r_1-R)\frac{\partial}{\partial r_1}+\frac{1}{2}\delta(r_2-R)\frac{\partial}{\partial r_2}, \tag{20}$$

where R is the box size and the Bloch operators $(1/2)\delta(r_\alpha-R)(\partial/\partial r_\alpha)$ ensure the Hermiticity of $\mathcal{H}_R$. The ionization cross sections are calculated as a sum over all the excitation cross sections to positive energy states of the basis in which $\mathcal{H}_R$ is diagonalized to obtain the R matrix. The R matrix is related to the K and J matrices, which are then used to determine the S matrix. In this study, the excitation cross section from state i to state f is given by

$$\sigma_{i\to j}(E)=\frac{\pi}{k_i^2}|S_{ij}-\delta_{ij}|^2. \tag{21}$$

For electron-impact scattering from hydrogen, we used a 2400-point lattice with a uniform mesh spacing of $\delta r=0.025$ and a box size of $R=60.0$ (a.u.).

III. RESULTS

A. Effect of using a model potential: $\frac{1}{r_1+r_2}$ versus $\frac{1}{r_>}$

In addition to the fully three-dimensional treatments, the problem of electron-impact scattering from hydrogen has been studied within simple s-wave models primarily to reduce the computational burden posed by solving the time-dependent Schrödinger equation in three dimensions. In one of these models, which was developed by Temkin [25] and Poet [26], the interaction potential between the electrons is

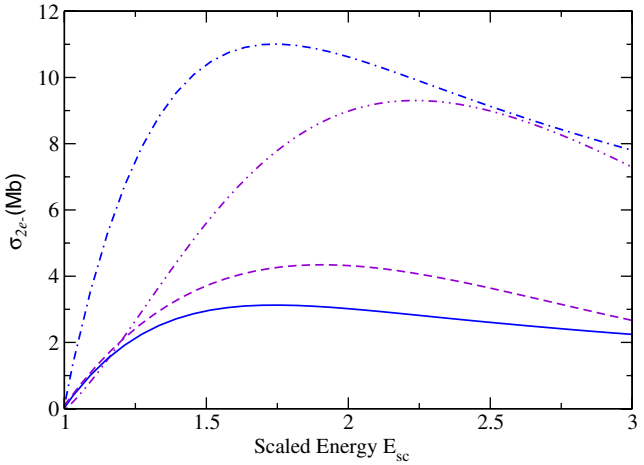

FIG. 2. (Color online) Ionization probability out of $n=1$ for H versus the scaled energy of the incoming electron from collinear s-wave DW (blue solid), Temkin-Poet DW (blue dot-dash), collinear s-wave RMPS (violet dash), and Temkin-Poet RMPS (violet dot-dot-dash) calculations. Note that the agreement between the DW and RMPS is better for the weaker collinear s-wave model potential. The data are fitted using least squares method to obtain the smooth curves.

described by the s-wave term of the partial wave expansion of the true electron-electron interaction potential, i.e., $1/|\vec{r}_1 - \vec{r}_2|$, and is $1/r_>$. The Temkin-Poet model has been used extensively in the literature for studying electron-impact scattering from hydrogen atoms (see, e.g., Refs. [24,27–30], and references therein). Our choice of the collinear s-wave model for studying electron-impact ionization stems from the fact that although the Temkin-Poet potential is exact for s waves, it was shown not to yield the correct threshold law in one dimension [19] due to its cusp along the $r_1=r_2$ ridge. This cusp weakly pushes the probability density away from the $r_1=r_2$ ridge resulting in distortion of the depicted threshold law. On the other hand, the collinear s-wave potential yields the correct threshold law.

One of the differences between the Temkin-Poet and the collinear models is that the collinear model potential is weaker than the exact s-wave potential of the Temkin-Poet model. As a consequence, the collinear DW method agrees very well with both TDCC and RMPS methods as demonstrated in the next two sections and Figs. 3 and 4. Due to the perturbative nature of the DW method, a weaker potential means better agreement with the nonperturbative methods.

To demonstrate this point, we have carried out DW and RMPS calculations for ionization from ground state of hydrogen within Temkin-Poet model and compared to the cross sections obtained using the collinear s-wave model. Results from these two calculations are shown in Fig. 2. The pseudoresonances in our RMPS data were smoothed out using a least squares fit to obtain the smooth RMPS curves in Fig. 2. As expected, there is better agreement between the DW and RMPS for the collinear s-wave model potential than in the case of the Temkin-Poet model potential. Cross sections for electron-impact ionization obtained using the Temkin-Poet potential are roughly a factor of 3 larger than those obtained using the model potential.

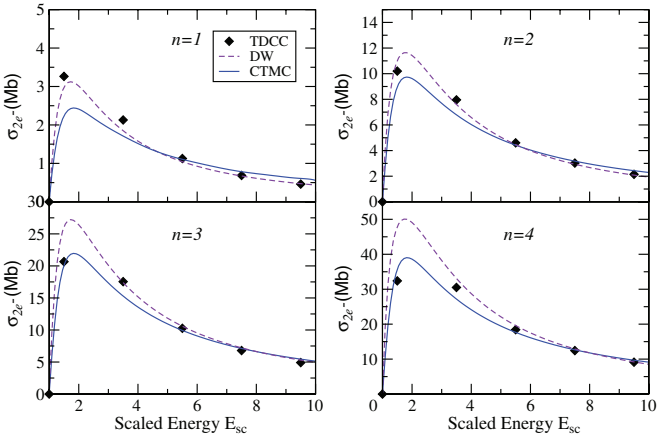

FIG. 3. (Color online) Ionization cross sections for $e^-+\mathrm{H}(^1S)$ scattering from n up to 4 calculated in collinear DW, CTMC, RMPS, and s-wave TDCC methods as a function of the scaled energy E_{sc} of the incoming electron.

B. Electron-impact ionization of hydrogen

Figure 3 shows electron-impact ionization cross sections from fully quantal collinear s-wave TDCC, DW, and CTMC calculations for up to $n=4$ of the hydrogen atom for the singlet symmetry of the initial wave packet. The CTMC result for $E_{sc}=1.5$ starts out ~44% off the TDCC result at $n=1$, then converges to the TDCC result by $n=4$. Note that the agreement between the CTMC and the TDCC methods gets better with the increasing electron-impact energy.

The collinear s-wave DW results are in good agreement with the collinear s-wave TDCC for the ground state ionization. For ionization out of states with higher n, DW results slowly diverge from both TDCC and CTMC cross sections. This observation is consistent with what has been seen from the fully three-dimensional calculations [13].

We have further carried out collinear s-wave RMPS calculations to serve as a benchmark for our TDCC results. We have observed reasonable agreement between the collinear s-wave RMPS and TDCC cross sections for all n we show in Fig. 3. This agreement can be considered to be an independent confirmation of the convergence of the TDCC results since both results are obtained via completely different quantal methods.

C. Electron-impact ionization of B^{4+}

Electron-impact ionization cross sections as a function of the scaled energy of the incoming electron from collinear s-wave DW, TDCC, and CTMC calculations are plotted for B^{4+} for initial states of $n=1$, 2, 4, and 8 in Fig. 4 for the ^1S symmetry. Cross sections from the CTMC calculations at $E_{sc}=1.5$ start out as ~74% larger than the TDCC cross sections at $n=1$, then very slowly converge to the TDCC results. For instance, at $n=8$ the CTMC result differs from the TDCC result by ~60% for scaled impact energy of 9.5. The agreement between the collinear s-wave TDCC and DW methods is excellent for all n plotted in Fig. 4. Despite being perturbative, DW works very well even for the highly excited states studied here because the interaction potential is

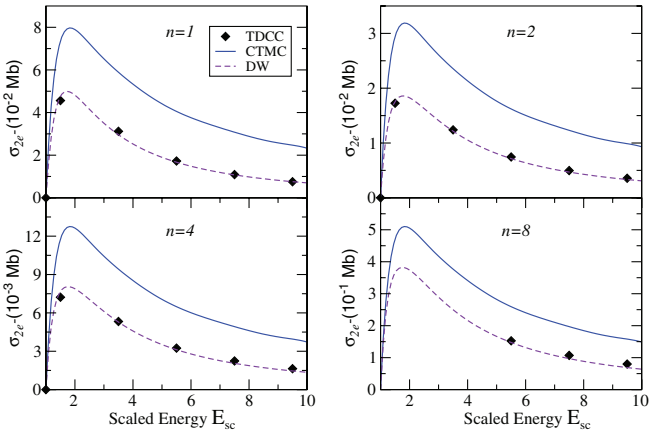

FIG. 4. (Color online) Ionization cross sections for $e^- - B^{4+}(^1S)$ scattering from $n=1$, 2, 4, and 8 calculated in collinear DW, CTMC, and *s*-wave TDCC methods as a function of the scaled energy of the incoming electron.

weak and the transition energy is large. The inelastic cross section to nearby n's are not as accurate due to the small energy spacing between Rydberg levels. Contrary to the case of hydrogen, both TDCC and DW results are below the classical cross sections.

It is expected that the results of the CTMC calculation would not be as close to the wave packet results as the H cross sections since higher nuclear charge manifests less classical behavior. Therefore, to see how high in n one should go for B^{4+} to reach agreement with the CTMC results, we have performed TDCC calculations for $n=1$, 2, 4, 8, 12, 16, 20, and 25 for the ^1S symmetry of the initial wave packet. The ionization probabilities versus the scaled energy of the incoming electron are plotted for all n in Fig. 5. The agreement between the CTMC and TDCC results improves substantially slower than it does for hydrogen as the principal quantum number n increases. For instance, for $n=25$, the CTMC results differ from the TDCC results by ~17% at $E_{sc}=5.5$ and by ~38% at $E_{sc}=9.5$.

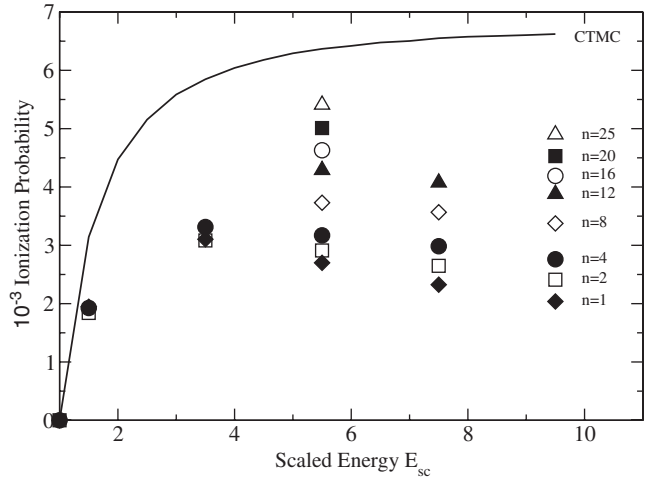

FIG. 5. CTMC versus *s*-wave TDCC method for the electron-impact ionization of B^{4+} for up to $n=25$ for the ^1S symmetry of the initial wave packet.

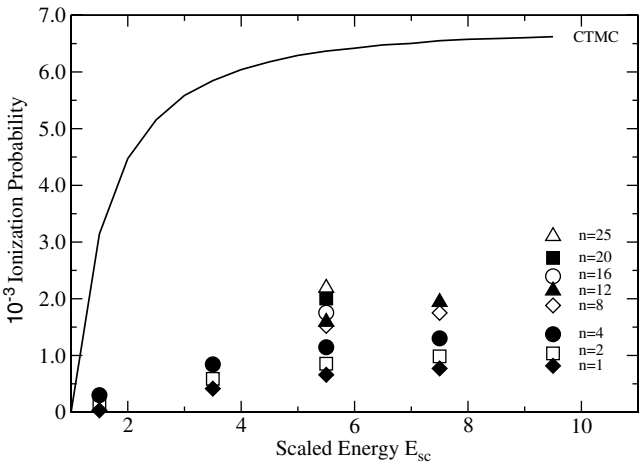

FIG. 6. CTMC versus *s*-wave TDCC method for the electron-impact ionization of B^{4+} for up to $n=25$ for the ^3S symmetry of the initial wave packet.

We have performed the same set of TDCC calculations for the ^3S symmetry of the initial wave packet and the results are seen in Fig. 6. Ionization probabilities for the ^3S symmetry are smaller than those for the ^1S symmetry as expected since the ^3S wave packet has a node along the $r_1=r_2$ ridge. The ^3S result from the TDCC calculation for $n=25$ at $E_{sc}=9.5$ is about a factor of 2 smaller than that from the CTMC calculation.

D. Effect of the ion stage

Since going from $Z=1$ to $Z=5$ drastically decreased the speed of convergence to the CTMC results as a function of n, we repeated the collinear *s*-wave TDCC calculation for an incoming electron with scaled energy of $E_{sc}=9.5$ for $Z=1$ through 6 for initial states with $n=1$, 2, 3, 4, 8, 12, 16, 20, and 25 to see the effect of the ion stage Z on the convergence speed of the quantal ionization probabilities to the classical ones as a function of n. In Fig. 7, we have plotted the ratio $P^{QM}(n,Z)/P^{CM}(Z)$ for the ^1S symmetry of the initial wave packet where $P^{QM}(n,Z)$ is the ionization probability from the

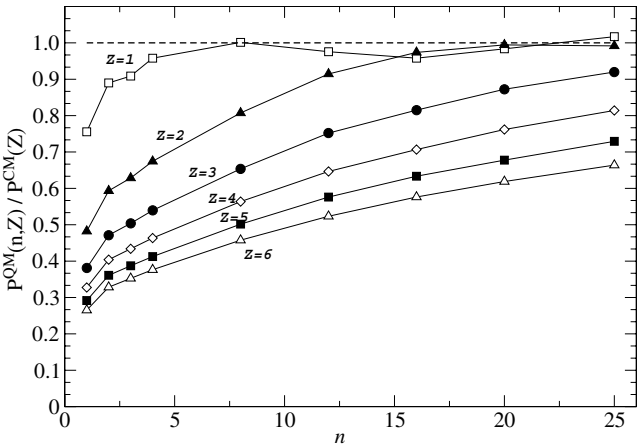

FIG. 7. Ratio of the quantal and classical ionization probabilities $P^{QM}(n,Z)/P^{CM}(Z)$, as a function of n for $Z=1-6$.

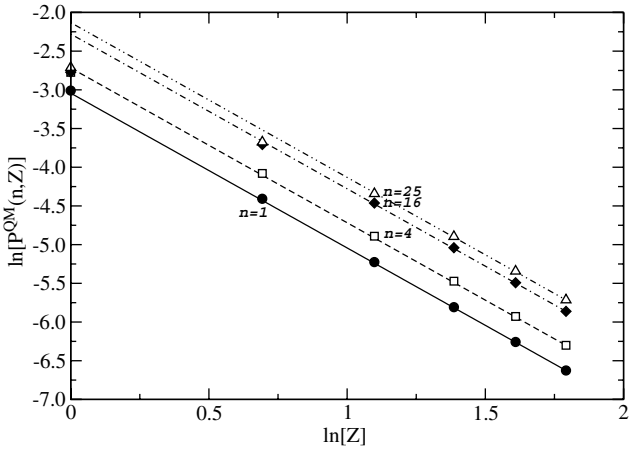

FIG. 8. $\ln[P^{QM}(n,Z)]$ versus $\ln(Z)$ for various n at $E_{sc}=9.5$. Note that the straight lines have a slope of 2 which implies $\sim 1/Z^2$ scaling of the ionization probability for $n=1$ and 4 and for higher Z of $n=16$ and 25.

TDCC calculation and $P^{CM}(Z)$ is the CTMC result. As noted before, for the case of $Z=1$ the TDCC method quickly converges to the CTMC result by $n=4$ within $\sim 4\%$ and by $n=8$ within $\lesssim 1\%$ for $E_{sc}=9.5$. The oscillations about the CTMC result for higher n are at the couple percent level and they may be due to the overall numerical accuracy of the TDCC method, although they may also be due to quantum interference.

Figure 8 shows $\ln[P^{QM}(n,Z)]$ versus $\ln(Z)$ for $n=1$, 4, 16, and 25 at the scaled electron-impact energy of $E_{sc}=9.5$. On top of the data points we have plotted lines of the form $2\ln(Z)+C$ where C is constant for each n line and evaluated so that the last data point for each n is fixed on its respective line. Note that for $n=1$ and 2 all the points lie on their lines whereas for the highest two ns the low Z substantially deviates from their respective lines. The fact that the slope of the lines is 2 means that for low n the ionization probability scales $\sim 1/Z^2$ and for high n it scales $\sim 1/Z^2$ only for the high Z.

E. Node structure near the scattering center

Looking at the classical trajectories that give rise to ionization, we can roughly estimate the size of the region where the energy exchange between the electrons takes place at the time of scattering from the core. To gain physical insight about the discrepancy between the classical and quantal results even for such high n, we may draw analogy to geometrical-wave optics correspondence. According to the geometrical-wave optics correspondence, light exhibits classical behavior when the wavelength is much smaller than the size of the region with which it interacts. In other words, we recover geometrical optics as the wave number gets larger within the interaction region. Applying the same idea to the matter waves, we can expect the system to behave more classically as the number of nodes increase in the region where classical energy exchange between the electrons takes place.

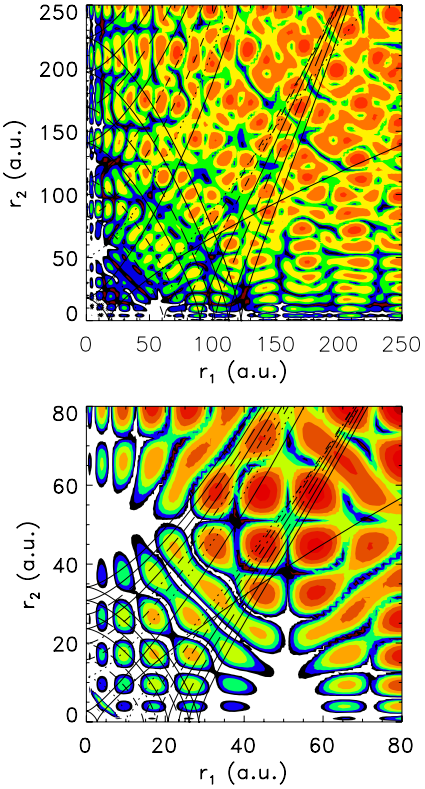

FIG. 9. (Color online) Contour plots for $|\psi_{n=16}(r_1,r_2)|^2$ for H (top panel) and B^{4+} (bottom panel) at the time of scattering from the nucleus at $E_{sc}=9.5$. The lines in each figure represent classical trajectories that lead to ionization.

The classical size of the scattering region that give ionization is $\ell_c \sim 0.1$ in scaled units (which is $L_c=2n^2\ell_c$) for $Z=5$ when the scaled energy of the incoming electron is 9.5. Using the Z-scaled potential, this characteristic size can be shown to be $L_c=51.2$ (a.u.) for $n=16$. For the lowest energy component in the wave function, the kinetic energy is approximately equal to the Z-scaled potential energy, i.e., $k^2/2 \sim 1/r$, from which $k(r) \sim \sqrt{2/r}$. We can use half wavelength in this energy regime to obtain a typical length scale of the region where the scattering takes place from the core. Half wavelength corresponding to $k(r)$ is

$$\pi \sim \int_0^{L_q} k(r)dr = \sqrt{8L_q} \tag{22}$$

from which $L_q \sim \pi^2/8 \simeq 1.2$. Comparing this with the classical size of the scattering region yields an intriguing result since the size of the classical scattering region is about a factor of 43 larger than the quantal length scale; therefore one would expect the quantal results to be in good agreement with the classical result at $n=16$.

In Fig. 9 we have plotted the absolute value square of the wave function for both $Z=1$ (top panel) and $Z=5$ (bottom panel) at $n=16$ for scaled energy $E_{sc}=9.5$. Various classical trajectories that give ionization are also plotted on top of each probability distribution. In these plots, we can define regions by using the points of the trajectories at which the coordinate of one electron vanishes, which we call bounce

points. Note that for $Z=1$, the number of nodes in the region bound by the last two bounces of the outmost classical trajectory is considerably larger than in the case of $Z=5$. For $Z=5$, Eq. (22) with $L_q \rightarrow L_c$ yields the number of nodes in the classical scattering region as $\sim\sqrt{8L_c}/\pi \sim 6$ which roughly equals the number of nodes in the bottom panel of Fig. 9 bounded by the last two bounces of the outmost classical trajectory.

IV. CONCLUSIONS

We have performed collinear *s*-wave time-dependent close-coupling (TDCC), classical trajectory Monte Carlo (CTMC), and distorted-wave (DW) calculations for electron-impact ionization of *H*-like ions with $Z=1-6$ for various principal quantum numbers up to $n=25$. We have observed good agreement between the *s*-wave TDCC and the CTMC methods for hydrogen as the principal quantum number reached $n=4$. The good agreement between the collinear *s*-wave TDCC and the classical results for hydrogen in the high-*n* limit is in accord with the expectations raised by the Bohr correspondence principle. Repeating the same set of calculations for B^{4+}, we have found that one has to go to much higher *n* for the collinear *s*-wave TDCC and the CTMC methods to agree. We showed that the TDCC results converge to the classical results very slowly with increasing *n*, which is in agreement with what Griffin *et al.* [13] have observed in their full three dimensional calculations up to $n=4$. At $n=25$ and for the ^1S symmetry of the initial wave packet, the TDCC method yields ionization probability which is $\sim$35% less than the classical result at the highest electron-impact energy we considered. For the same *n* and electron-impact energy, the TDCC result is about a factor of 2 less than the CTMC result for the ^3S case.

The collinear *s*-wave DW calculations for hydrogen resulted in cross sections which are in good agreement with the collinear *s*-wave TDCC calculations for the ground state, and gradually got worse as *n* is increased. In the case of B^{4+}, we have shown that the agreement between the DW and TDCC is excellent up to $n=8$. This suggests that, for the low lying excited states, the DW is just as good as the exact TDCC method, which makes it useful for the plasma modeling and diagnosing purposes. One would expect a perturbative method to work when only a small fraction of the initial state ionizes, leaving most of the initial population in the initial state. The fact that the collinear *s*-wave DW method works so well even though it is perturbative may be due to the small interaction potential compared to the ionization energy. The energy difference between the adjacent states decreases as $\sim 1/n^3$ for high *n* and the incoming electron can knock the atom into a nearby *n* state instead of ionizing it. This is even more probable for the model potential we used, which is weaker than the actual $1/|\vec{r}_{12}|$ potential.

To illustrate the effect of the ion state *Z* on the ionization probabilities, we have carried out collinear *s*-wave TDCC calculations for *Z* up to 6 and for *n* up to 25 at the scaled electron-impact energy $E_{sc}=9.5$. We found that for low-*n* the ionization probability scales as $\sim 1/Z^2$ and for high-*n* it behaves the same only for high *Z*.

In order to understand the physical size scales involved and gain some insight on the dynamics behind this slowly converging behavior, we drew analogy to geometrical-wave optics correspondence and estimated the number of nodes in the region near the core outlined by the classical trajectories that give ionization. We have found that the size of the classical scattering region is about a factor of 50 larger than the quantal length scale; therefore, one would expect the TDCC and CTMC methods to agree, which is not in accord with what we have observed. The peculiar dynamics behind this slow convergence is intriguing and may be due to an inherent characteristic of the line-land potential or a quantum interference effect.

ACKNOWLEDGMENTS

This work was supported by the Office of Basic Energy Sciences and the Office of Fusion Energy Sciences, U.S. Department of Energy.

[1] L. S. Brown, Am. J. Phys. **41**, 525 (1973).
[2] B. Gao, Phys. Rev. Lett. **83**, 4225 (1999).
[3] A. J. Makowski and K. J. Górska, Phys. Rev. A **66**, 062103 (2002).
[4] J. A. Yeazell and C. R. Stroud, Phys. Rev. Lett. **60**, 1494 (1988).
[5] K. Nagesha and K. B. MacAdam, Phys. Rev. Lett. **91**, 113202 (2003).
[6] H. Deutsch, K. B. MacAdam, K. Becker, H. Zhang, and T. D. Märk, J. Phys. B **39**, 343 (2006).
[7] Philip L. Bartlett and Andris T. Stelbovics, Phys. Rev. A **69**, 040701(R) (2004).
[8] D. Vrinceanu, Phys. Rev. A **72**, 022722 (2005).
[9] M. A. Uddin, A. K. F. Haque, A. K. Basak, K. R. Karim, and B. C. Saha, Phys. Rev. A **72**, 032715 (2005).
[10] K. Bartschat and I. Bray, J. Phys. B **29**, L577 (1996).
[11] M. C. Witthoeft, S. D. Loch, and M. S. Pindzola, Phys. Rev. A **70**, 022711 (2004).
[12] J. Colgan, S. D. Loch, M. S. Pindzola, C. P. Ballance, and D. C. Griffin, Phys. Rev. A **68**, 032712 (2003).
[13] D. C. Griffin, C. P. Ballance, M. S. Pindzola, F. Robicheaux, S. D. Loch, J. A. Ludlow, M. C. Witthoeft, J. Colgan, C. J. Fontes, and D. R. Schultz, J. Phys. B **38**, L199 (2005).
[14] H. P. Summers, N. R. Badnell, M. G. O'Mullane, A. D. Whiteford, R. Bingham, B. J. Kellett, J. Lang, K. H. Behringer, U. Fantz, K-D Zastrow, S. D. Loch, M. S. Pindzola, D. C. Griffin, and C. P. Ballance, Plasma Phys. Controlled Fusion **44**, B323 (2002).
[15] S. D. Loch, C. J. Fontes, J. Colgan, M. S. Pindzola, C. P. Ballance, D. C. Griffin, M. G. O'Mullane, and H. P. Summers, Phys. Rev. E **69**, 066405 (2004).
[16] J. M. Rost, Phys. Rev. Lett. **72**, 1998 (1994).

[17] Gerd van de Sand and Jan M. Rost, J. Phys. B **33**, 1423 (2000).
[18] G. H. Wannier, Phys. Rev. **90**, 817 (1953).
[19] F. Robicheaux, M. S. Pindzola, and D. R. Plante, Phys. Rev. A **55**, 3573 (1997).
[20] M. S. Pindzola and F. Robicheaux, Phys. Rev. A **55**, 4617 (1997).
[21] M. C. Witthoeft, M. S. Pindzola, and J. Colgan, Phys. Rev. A **67**, 032713 (2003).
[22] F. Robicheaux, E. Oks, A. L. Parker, and T. Uzer, J. Phys. B **35**, 4613 (2002).
[23] J. Botero and J. H. Macek, J. Phys. B **24**, L405 (1991).
[24] M. S. Pindzola, D. Mitnik, and F. Robicheaux, Phys. Rev. A **62**, 062718 (2000).
[25] A. Temkin, Phys. Rev. **126**, 130 (1962).
[26] R. Poet, J. Phys. B **11**, 3081 (1978).
[27] P. L. Bartlett and A. T. Stelbovics, Phys. Rev. A **69**, 022703 (2004).
[28] P. L. Bartlett, I. Bray, S. Jones, A. T. Stelbovics, A. S. Kadyrov, K. Bartschat, G. L. Ver Steeg, M. P. Scott, and P. G. Burke, Phys. Rev. A **68**, 020702(R) (2003).
[29] A. Temkin and Y. Hahn, Phys. Rev. A **9**, 708 (1974).
[30] S. Jones and A. T. Stelbovics, Phys. Rev. A **66**, 032717 (2002).